Vertical Transmission of Bovine H5N1 during Pregnancy and Lactation in Mice

Brittany A. Seibert[1†], Maclaine A. Parish[1†], Sattya N. Talukdar[1], Tianle Zhang[1], Sabal Chaulagain[1], Jennifer A. Liu[1], Jaiprasath Sachithanandham[1], Cosette Schneider[2], Lynda Coughlan[2,3], Andrew S. Bowman[4], Richard J. Webby[5], Jack R. Harkema[6], Andrew Pekosz[1], Sabra L. Klein[1*]

Affiliations:

[1]W. Harry Feinstone Department of Molecular Microbiology and Immunology, Johns Hopkins Bloomberg School of Public Health, Baltimore, MD, USA

[2]Department of Microbiology and Immunology, University of Maryland School of Medicine, Baltimore, MD, USA

[3]Centre for Vaccine Development and Global Health (CVD), University of Maryland School of Medicine, Baltimore, MD, USA

[4]Department of Veterinary Preventive Medicine, The College of Veterinary Medicine, The Ohio State University, Columbus, OH, USA

[5]Department of Host-Microbe Interactions, St. Jude Children's Research Hospital, Memphis, TN, USA

[6]Department of Pathobiology and Diagnostic Investigation, Michigan State University, East Lansing, MI, USA

*Correspondence: Sabra Klein, sklein2@jhu.edu

†Authors contributed equally to this work; Author order reflects relative contribution.

Abstract

Panzootic spillover of H5N1 virus clade 2.3.4.4b has resulted in expanded host range among placental mammals, with lactation transmission via milk documented. Whether infection during pregnancy leads to *in utero* or lactational vertical transmission remains unknown. Pregnant outbred mice were infected with A/bovine/Ohio/B24OSU-472/2024 during the second or third trimester equivalent. Second trimester infection caused *in utero* infection, with infectious virus detected in the uterus, placenta, and fetus. Birth following third trimester infection resulted in offspring with decreased size and neurodevelopmental delays, with infectious virus detected in the neonatal milk ring and lungs as well as mammary tissues. Ongoing H5N1 infections present increased risk for human exposure and an H5N1 vertical transmission model in placental mammals is essential for understanding viral spread and evaluating treatments during pregnancy.

Main Text:

The evolving ecology of highly pathogenic avian influenza (HPAI) H5N1 involves increased mammalian infections. The outbreak of HPAI H5N1 clade 2.3.4.4b in U.S. dairy cattle, likely resulted from a single introduction of the B3.13 genotype virus from birds, followed by sustained transmission among cattle (*1, 2*). Viral RNA is detected in the milk and mammary tissue of dairy cattle, and experimental ingestion of contaminated milk in mice causes fatal systemic infection (*3, 4*). Ongoing transmission of HPAI H5N1 among dairy cattle and its spillover to other mammalian species increases the risk of human exposure.

While there are currently no reports of HPAI H5N1 clade 2.3.4.4b in pregnant women from this outbreak, pregnant women have historically been at greater risk of severe disease and death following infection with HPAI as well as seasonal and pandemic influenza A viruses (*5, 6*). An analysis of 30 pregnant women diagnosed with avian influenza virus infection (H5N1, H5N6, and H7N9) reported that more than half were infected with H5N1, which occurred across gestational ages, with all but two resulting in maternal and *in utero* fetal death (*5*). Pregnant mice infected with a 2006 H5N1 (clade 2.3.4) had detectable viral RNA in both placental and fetal tissues (*7*). Despite poor maternal and infant outcomes, there is limited information on the pathogenesis of HPAI during pregnancy.

Pregnancy represents a distinct physiological and immunological state, which causes more severe outcomes from influenza infections than non-pregnant individuals (*5, 6*). The bovine H5N1 outbreak, including reports of fatal infections in cats on affected farms (*8*), multiple infections among dairy farm workers (*9, 10*), and a pediatric H5N1 case (*11, 12*), emphasizes the public health risk and heightened potential for household exposure among pregnant women. While a previous study demonstrated that bovine H5N1 inoculation of post-birth lactating female mice can result in transmission of virus to offspring through milk (*3*), it remains unknown whether *in utero* transmission of bovine H5N1 viruses occurs. Recent reports on cattle farms indicate that H5N1-infected heifers exhibit reproductive complications, including abortions during mid- to late-gestation, and a reduced number of cattle in estrus during periods of high clinical disease (*13, 14*). We have established a pregnancy mouse model to study the pathogenesis and transmission dynamics of bovine H5N1from the 2024 outbreak.

H5N1 dissemination and pathogenesis in non-pregnant and pregnant female mice

We examined the pathogenesis of two B3.13 genotype bovine isolates, A/bovine/Texas/98638/2024 (H5N1; A/bovine/TX) and A/bovine/Ohio/B24OSU-439/2024 (H5N1; A/bovine/OH) in non-pregnant outbred female mice. We utilized outbred mice because they better approximate the tolerogenic immune responses required to prevent rejection of semi-allogeneic fetuses (*15*), and exhibit improved survival following pandemic H1N1 challenge compared with inbred strains (*15-17*). We intranasally inoculated non-pregnant females with 100 TCID50 of A/bovine/TX, A/bovine/OH H5N1, or media. Similar morbidity was observed for both viruses (**Fig. S1A-B**). Peak clinical signs of disease appeared earlier in mice infected with A/bovine/TX (5 days post-infection [dpi]) compared to those infected with A/bovine/OH (9 dpi) (**Fig. S1C**). All mice infected with A/bovine/TX succumbed by 6 dpi, while those infected with A/bovine/OH succumbed by 9 dpi (**Fig. S1D**). At 5 dpi, females infected with A/bovine/TX exhibited greater infectious viral loads in the nasal turbinates, mammary glands, ovaries, and nervous system tissues than females infected with A/bovine/OH (**Fig. S1E**). Similar viral loads were detected in whole blood, trachea, lungs, and colon. We selected A/bovine/OH for subsequent experiments in pregnant mice to increase the probability of survival. When we

infected non-pregnant mice with a lower dose of A/bovine/OH, although not statistically significant, mice infected with 10 TCID50 of A/bovine/OH showed reduced morbidity and mortality compared to those infected with 100 TCID50 (**Fig. S1F-G**).

We intranasally inoculated pregnant mice (dams) with either 10 or 100 TCID50 of A/bovine/OH at embryonic day (E)10, roughly corresponding to the human second trimester (*15, 18*). Rectal temperature indicated that the inoculation dose, more than pregnancy status, influenced morbidity (**Fig. 1A**). Both pregnant and non-pregnant mice given 100 TCID50 showed greater hypothermia compared to those given 10 TCID50. At 6 dpi, non-pregnant females showed greater viral loads in both nasal turbinates and lungs. Pregnant mice, particularly those receiving 100 TCID50, showed greater detectable infectious virus in the ovaries and uterus (**Fig. 1B**). Among females receiving the 100 TCID50 dose, infectious virus was detected in the ovaries and in at least one uterine horn in 6/6 pregnant mice, compared to infectious virus being detected in the ovaries and/or uterine horns of only 2/5 non-pregnant mice.

Histological examination of the lungs in the pregnant females infected with 100 TCID50 of A/bovine/OH revealed viral protein localized in luminal epithelial cells lining distal preterminal and terminal bronchioles and centriacinar alveoli (**Fig. 1C**). Pulmonary histopathology was greater in pregnant mice infected with 100 TCID50 compared to those infected with 10 TCID50 or mock-infected (**Fig. 1D**). While no histopathology was present in the lungs of mock-infected mice, there was moderate to severe pulmonary histopathology in infected mice, that was characterized by a locally extensive to widespread subacute necrotizing alveolitis and bronchiolitis (**Fig. 1E**). Infected lungs had virus-induced apoptosis, necrosis, and exfoliation of airway epithelium lining distal, small-diameter bronchioles extending to terminal bronchioles in the centriacinar regions of the lung. Bronchiolar epithelial lesions were accompanied by an acute to subacute mixed inflammatory cell infiltrate composed of neutrophils and mononuclear cells (lymphocytes and monocytes) along with intramural and luminal accumulation of proteinaceous fluid (**Fig. 1E, arrows**). Epithelial and inflammatory cell lesions extended into alveolar ducts and alveoli characterized by a necrotizing and exudative alveolitis with scattered focal areas of apoptotic epithelial cells and apoptotic bodies lining alveolar septa, and accumulation of mixed inflammatory cells and proteinaceous fluid in alveolar airspaces (**Fig. 1E**).

In utero vertical transmission of bovine H5N1

To determine whether *in utero* vertical transmission occurred, placental and fetal tissues were examined for infectious virus at 6 dpi. Among pregnant females infected with 10 TCID50, 2/7 litters (11 of 42 conceptuses [comprising the uterus, placenta, and fetus]) had detectable infectious virus in the placenta, with one litter also showing corresponding viral detection in the fetuses (4 of 42 conceptuses) (**Fig. 2A**). Dams infected with 100 TCID50 had infectious virus detected in 6/6 litters (31 of 34 conceptuses), with three litters also exhibiting infectious virus in the fetuses (13 of 34 conceptuses), suggesting dose-dependent increased virus prevalence in the placenta and transmission to fetal tissues.

No histopathology was present in the placenta of mock-infected pregnant mice. For the embryonic age of the dams at the time of tissue collection (E16), there was an expected amount of degeneration and subsequent necrosis in the maternal decidua in mock dams and only slightly more decidual and junctional zone deterioration in H5N1-infected dams. In a subset of placentas from infected dams, virus-associated, small focal lesions were observed scattered within the labyrinth layer (**Fig. 2B**). These lesions consisted of trophoblasts with nuclear inclusions or

apoptotic cell death features, e.g., pyknosis, karyorrhexis, apoptotic bodies and phagocytic cells containing cellular debris. Virus-associated histopathological changes were observed in the columnar epithelial cells lining the yolk sac (**Fig. 2C, arrow**).

Immunofluorescence staining for H5N1 antigen was utilized to identify the spatial distribution of the virus. No viral protein was observed in placentas collected from mock-infected dams (**Fig. 2D**). Placentas from dams infected with 10 (**Fig. S2A**) or 100 (**Fig. 2E**) TCID50 displayed viral protein localized to the decidua, junctional zone, and labyrinth zone, consistent with the distribution of virus-associated lesions noted in the labyrinth zone. We evaluated the distribution of viral protein in fixed conceptuses to examine viral distribution in tissues disrupted during the dissection process. Viral antigen was absent in the mock-infected dams (**Fig. 2F**), but was detected in the yolk sac of a conceptus from one dam infected with 100 TCID50 (**Fig. 2G**). Because the yolk sac plays a key role in fetal nutrition (*19*), we evaluated placental and fetal mass at 6 dpi. Maternal H5N1 infection at E10 results in significantly decreased placental but not fetal mass (**Fig. S3**). Because infectious virus was detected in a subset of fetuses without growth restriction at either dose, we examined the localization of viral protein in fixed fetuses from litters that exhibited vertical transmission. This provided a more comprehensive evaluation, as fetal orientation in fixed conceptuses can obscure the sagittal plane. Viral protein, absent in fetuses from mock-infected dams (**Fig. 2H**), was localized in the intestinal tissue of fetuses from dams infected with either 10 (**Fig. S2B**) or 100 (**Fig. 2I**) TCID50.

Vertical transmission of bovine H5N1 post-birth

To investigate post-birth virus transmission, pregnant mice were inoculated with 10 or 100 TCID50 of A/bovine/OH during the human third trimester equivalent (E16) (*15, 18*). Dams, along with their entire litter, were euthanized at 1 or 4 days post-birth (dpb), corresponding to 4 or 7 dpi. Compared to dams infected with 10 TCID50, those infected with 100 TCID50 exhibited reduced morbidity, along with increased clinical signs of disease before the study endpoint (**Fig. S4**). At 4 dpi (1 dpb), only 2/5 litters from dams infected with 100 TCID50 had detectable virus in at least one of the pups' lungs and /or milk ring, while virus was undetectable in all litters from dams infected with 10 TCID50 (**Fig. 3A**). We evaluated viral dissemination in milk and four distinct mammary glands (*20*). At 7 dpi (4 dpb), a subset of dams infected with 10 (3/6) or 100 (3/6) TCID50 had detectable virus in their lungs and mammary tissue (**Fig. 3B**). Infectious virus was detected in at least one of the pups' lungs and/or milk ring from 1/6 dams infected with 10 TCID50 and 2/6 dams infected with 100 TCID50. Pups with detectable infectious virus were born to dams that also had virus detected in the milk and inguinal mammary tissue.

We determined whether the presence of H5N1 in mammary tissues resulted in pathological changes at 7 dpi (4 dpb). No histopathology was present in any of the lactating mammary glands of mock-infected dams (**Fig. 3C**). Terminal acinar lumens in the mock-infected dams contained a mixture of lipid and proteinaceous material, and the epithelial cells lining the lumens exhibited marked cytoplasmic vacuolation due to the presence of secretory lipid droplets. The terminal acinar lumens in the mammary glands of H5N1-infected dams were noticeably less distended and contained proteinaceous material, and exfoliated epithelial cells, with some cells exhibiting pyknotic or karyorrhectic nuclei (**Fig. 3C, arrows**). Basophilic regenerative epithelium predominantly lined the acinar lumens of the H5N1-infected mice. When examining the presence of viral antigen by immunohistochemistry, cytoplasmic and nuclear staining of the N1 protein was observed in the epithelial cells lining the terminal acinar lumens for dams infected with either 10 (**Fig. S5**) or 100 (**Fig. 3C**) TCID50.

To further evaluate vertical transmission at later timepoints during lactation, dams were only inoculated with 10 TCID50 A/bovine/OH at E16 to increase survival. Tissues from subsets of pups within individual litters were examined for infectious virus 1- 25 dpb, which corresponded to 4-28 dpi. Infected dams did not exhibit changes in morbidity, but clinical signs of disease peaked at 9 dpi (**Fig. S4**). Between 7 and 9 dpi, virus was detected in the lungs, mammary glands, and milk in a subset of dams (**Fig. 4A**), whereas no virus was detected in tissues collected from dams euthanized at 28 dpi (**Fig. 4B**). While no pups had detectable virus at 1 dpb (4 dpi), virus was detected in the milk ring, lungs, and blood from pups at 4 dpb (7 dpi) and 6 dpb (9 dpi) (**Fig. 4C**). In contrast, no virus was detected in pups at either 12 dpb (15 dpi) or 25 dpb (28 dpi).

To confirm that dams and pups at 25 dpb (28 dpi) were infected, antibody responses to H5N1 were measured. H5- and N1-specific IgG and IgM titers were detectable in both dams euthanized at 28 dpi (**Fig. 4D-F**). While the pups from the dams euthanized at 28 dpi did not have infectious virus, a subset of pups had detectable H5- and N1- specific IgG titers, suggesting either transfer of maternal antibodies or possible infection (**Fig. 4D**). High titers of H5-specific IgG1, IgG2a, IgG2b, IgG2c, and IgG3 were detected in dams and pups, with N1-specific antibodies predominantly comprised of IgG2a, IgG2b, and IgG2c subclasses (**Fig. S6**). Only one pup from each litter had detectable IgA (**Fig. 4E**). Detectable H5- and N1-specific IgM were detected in one pup from each litter, suggesting a de novo immune response (**Fig. 4F**).

Postnatal outcomes following maternal bovine H5N1 infection

To determine adverse developmental outcomes from maternal H5N1 infection, litters from pregnant females infected with either 10 or 100 TCID50 of A/bovine/OH at E16 were evaluated. Infection with either dose of H5N1 did not impact litter size (**Fig. S7A**) or cause pre-term birth (**Fig. S7B**). H5N1 infection of dams resulted in growth restriction in pups, as indicated by their smaller birth weight (**Fig. S7C**), shorter body length (**Fig. S7D**), and smaller head diameter (**Fig. S7E**). Because dams infected with 100 TCID50 were euthanized by 7 dpi due to increased morbidity (**Fig. S5A–C**), neurodevelopmental assessments were only conducted on pups from dams infected with 10 TCID50. At 5 dpb, cliff aversion (**Fig. 4G**), measuring vestibular function, negative geotaxis (**Fig. 4H**), measuring sensorimotor competence and vestibular function, and surface righting (**Fig. 4I**), measuring motor development, were delayed in offspring of H5N1- compared to mock-infected dams and persisted at 9 dpb (**Fig. 4J-L**).

Discussion

We developed a model to study bovine H5N1 pathogenesis during pregnancy and observed distinct tissue tropism, with elevated viral titers in the reproductive tissues of pregnant mice. We showed *in utero* vertical H5N1 transmission following intranasal inoculation of outbred pregnant mice at E10, as indicated by infectious virus in placental and fetal tissues with viral protein localization in labyrinth zone, the yolk sac, and fetal intestines. Dams infected at E16 also transmitted virus to pups post-birth, most likely via milk, resulting in both acute and long-lasting adverse perinatal and developmental outcomes. These results provide insights into the vertical transmission dynamics of bovine H5N1 and contribute to the risk assessment of a high-risk population.

Infection during the second trimester (E10) of pregnancy reflects case studies that analyzed tissues from H5N1-positive patients (*5, 21*). We observed reduced placental mass with minimal placental pathology and no significant change in fetal mass. Analysis of a woman at 4 months of gestation who succumbed to H5N1 infection revealed normal placental development

corresponding to gestational age and no histopathological abnormalities in fetal tissue (*21*). Acute necrotizing deciduitis, also observed in our mouse model, was identified in the placenta of the pregnant woman (*21*). Although placental and fetal damage was minimal, the woman exhibited widespread pulmonary damage (*21*), consistent with our findings. When examining viral RNA or protein, the placental tissue from the pregnant woman showed infected cells in the chorionic villi, with viral RNA in the lungs and liver of the fetus (*21*). We observed viral protein in the placental labyrinth zone. Both the mouse labyrinth and human chorionic villi are sites of maternal-fetal gas and nutrient exchange and are considered homologous structures (*22*). Infection of inbred dams with A/Shenzhen/406H/2006 (clade 2.3.4) at E10 resulted in detectable viral RNA in both placental and fetal tissues with no analysis of anatomical distribution of virus (*7*). In our model, viral protein was detected within the intestines of fetuses from H5N1-infected dams. We hypothesize fetuses may have ingested virus-containing amniotic fluid, which peaks during mid-to-late gestation and is critical for fetal intestinal development (*23*). A previous human case of H5N1 infection during pregnancy reported intra-amniotic infection (*24*).

There are high levels of viral RNA or protein in milk and mammary tissue, accompanied by decreased milk production, and milk with a thickened, yellow-colored appearance in infected cattle (*8, 25*). Experimental intra-mammary infection in dairy cattle results in high viral loads in milk and infected udder quarters with limited local spread (*26, 27*). Viral antigen in the mammary tissue from inoculated quarters was detected in alveolar epithelial cells and was associated with alveolar shrinkage lined by swollen epithelial cells, and replacement of secretory alveoli with fibrous connective tissue (*26*). This is consistent with our observation of viral antigen in the epithelial cells lining the secretory alveoli of infected mammary tissue following intranasal inoculation. Whether these pathological changes are due to virus-induced pathology or a consequence of decreased milk production leading to mammary tissue reduction requires further study.

Given reports of fatal systemic influenza in cats and mice following ingestion of unpasteurized colostrum or milk from infected dairy cattle (*3, 4, 8*), we also used this late-gestation infection model to investigate the transmission window of bovine H5N1 during lactation. Consistent with a previous study of H5N1 infected lactating BALB/c female mice (*3*), we observed infectious virus in pups from infected pregnant mice at 7–9 dpi, corresponding to 4–6 dpb. Also consistent with the findings by Eisfeld et al., we observed detectable infectious virus in pups from 2 of 5 litters born to dams infected with 100 TCID50 at 7 dpi (4 dpb) (*3*). To date, no studies have examined offspring development following maternal H5N1 infection, whether acquired *in utero* or postnatally. We observed that H5N1 infection during pregnancy results in intrauterine growth restriction and offspring with neurodevelopmental delays, consistent with effects of H1N1 infection during pregnancy (*15, 28*).

H5N1 clade 2.3.4.4b has spread among numerous placental mammals, heightening concerns about their zoonotic potential amid repeated introductions to dairy cattle. In addition to the infections in barn cats (*8*) on affected farms and multiple infected dairy farm workers (*9*), a recent report documented H5N1 infection in indoor domestic cats from households of dairy workers employed on farms positive for H5N1 (genotype B3.13) (*29*). Although the current public health risk of H5N1 remains low, potential exposure and transmission, such as fomites, from individuals working with infected cattle or poultry to household pets and family members is possible. These results provide the groundwork for understanding the vertical transmission of bovine H5N1 viruses in humans and other placental mammals, including cattle, where adverse pregnancy outcomes have recently been reported following H5N1 infection (*13, 14*).

References and Notes

1. A. C. Lowen *et al.*, Pandemic risk stemming from the bovine H5N1 outbreak: an account of the knowns and unknowns. *J Virol* **99**, e0005225 (2025).
2. T. Q. Nguyen *et al.*, Emergence and interstate spread of highly pathogenic avian influenza A(H5N1) in dairy cattle in the United States. *Science* **388**, eadq0900 (2025).
3. A. J. Eisfeld *et al.*, Pathogenicity and transmissibility of bovine H5N1 influenza virus. *Nature* **633**, 426-432 (2024).
4. L. Guan *et al.*, Cow's Milk Containing Avian Influenza A(H5N1) Virus - Heat Inactivation and Infectivity in Mice. *N Engl J Med* **391**, 87-90 (2024).
5. R. Purcell, M. L. Giles, N. W. Crawford, J. Buttery, Systematic Review of Avian Influenza Virus Infection and Outcomes during Pregnancy. *Emerg Infect Dis* **31**, 50-56 (2025).
6. P. S. Creisher, S. L. Klein, Pathogenesis of viral infections during pregnancy. *Clin Microbiol Rev* **37**, e0007323 (2024).
7. L. Xu, L. Bao, W. Deng, C. Qin, Highly pathogenic avian influenza H5N1 virus could partly be evacuated by pregnant BALB/c mouse during abortion or preterm delivery. *Virol J* **8**, 342 (2011).
8. E. R. Burrough *et al.*, Highly Pathogenic Avian Influenza A(H5N1) Clade 2.3.4.4b Virus Infection in Domestic Dairy Cattle and Cats, United States, 2024. *Emerg Infect Dis* **30**, 1335-1343 (2024).
9. CDC, H5 Bird Flu: Current Situation. *Avian Influenza (Bird Flu)*, (2025).
10. T. M. Uyeki *et al.*, Highly Pathogenic Avian Influenza A(H5N1) Virus Infection in a Dairy Farm Worker. *N Engl J Med* **390**, 2028-2029 (2024).
11. CDC, CDC confirms H5N1 Bird Flu Infection in a Child in California. *CDC Newsroom*, (2024).
12. CDC, Technical Update: Summary Analysis of the Genetic Sequence of a Highly Pathogenic Avian Influenza A(H5N1) Virus Identified in a Child in California. *Avian influenza (Bird Flu)*, (2024).
13. B. A. Petersen, High-Pathogenicity (Highly Pathogenic) Avian Influenza in Cattle. *Merck Manual*, (2025).
14. R. Brooks, Some California Veterinarians Say Virus-Hit Dairies See More Abortions in First-Calf Heifers and Dry Cows. *Bovine Veterinarian*, (2025).
15. P. S. Creisher *et al.*, Suppression of progesterone by influenza A virus mediates adverse maternal and fetal outcomes in mice. *mBio* **15**, e0306523 (2024).
16. K. J. McHugh, S. Mandalapu, J. K. Kolls, T. M. Ross, J. F. Alcorn, A novel outbred mouse model of 2009 pandemic influenza and bacterial co-infection severity. *PLoS One* **8**, e82865 (2013).
17. M. S. Vermillion *et al.*, Pregnancy preserves pulmonary function following influenza virus infection in C57BL/6 mice. *Am J Physiol Lung Cell Mol Physiol* **315**, L517-L525 (2018).
18. J. L. Sones, R. L. Davisson, Preeclampsia, of mice and women. *Physiol Genomics* **48**, 565-572 (2016).
19. A. Ornoy, R. K. Miller, Yolk sac development, function and role in rodent pregnancy. *Birth Defects Res* **115**, 1243-1254 (2023).
20. E. Honvo-Houeto, S. Truchet, Indirect Immunofluorescence on Frozen Sections of Mouse Mammary Gland. *J Vis Exp*, (2015).
21. J. Gu *et al.*, H5N1 infection of the respiratory tract and beyond: a molecular pathology study. *Lancet* **370**, 1137-1145 (2007).
22. M. Rusidze *et al.*, Estrogen Actions in Placental Vascular Morphogenesis and Spiral Artery Remodeling: A Comparative View between Humans and Mice. *Cells* **12**, (2023).
23. M. A. El-Haddad, M. Desai, D. Gayle, M. G. Ross, In utero development of fetal thirst and appetite: potential for programming. *J Soc Gynecol Investig* **11**, 123-130 (2004).
24. T. V. Le *et al.*, Fatal avian influenza A(H5N1) infection in a 36-week pregnant woman survived by her newborn in Soc Trang Province, Vietnam, 2012. *Influenza Other Respir Viruses* **13**, 292-297 (2019).
25. L. C. Caserta *et al.*, Spillover of highly pathogenic avian influenza H5N1 virus to dairy cattle. *Nature* **634**, 669-676 (2024).
26. A. L. Baker *et al.*, Dairy cows inoculated with highly pathogenic avian influenza virus H5N1. *Nature* **637**, 913-920 (2025).
27. N. J. Halwe *et al.*, H5N1 clade 2.3.4.4b dynamics in experimentally infected calves and cows. *Nature* **637**, 903-912 (2025).
28. J. Y. Song *et al.*, Paradoxical long-term impact of maternal influenza infection on neonates and infants. *BMC Infect Dis* **20**, 502 (2020).
29. Ramya Naraharisetti *et al.*, Highly Pathogenic Avian Influenza A(H5N1) Virus Infection of Indoor Domestic Cats Within Dairy Industry Worker Households — Michigan, May 2024. *Morbidity and Mortality Weekly Report (MMWR)*. 2025.

30. N. J. Swanson *et al.*, 2019-2020 H1N1 clade A5a.1 viruses have better in vitro fitness compared with the co-circulating A5a.2 clade. *Sci Rep* **13**, 10223 (2023).
31. L. G. vom Steeg *et al.*, Androgen receptor signaling in the lungs mitigates inflammation and improves the outcome of influenza in mice. *PLoS Pathog* **16**, e1008506 (2020).
32. L. G. vom Steeg *et al.*, Age and testosterone mediate influenza pathogenesis in male mice. *Am J Physiol Lung Cell Mol Physiol* **311**, L1234-L1244 (2016).
33. E. J. DePeters, R. C. Hovey, Methods for collecting milk from mice. *J Mammary Gland Biol Neoplasia* **14**, 397-400 (2009).
34. D. N. Feather-Schussler, T. S. Ferguson, A Battery of Motor Tests in a Neonatal Mouse Model of Cerebral Palsy. *J Vis Exp*, (2016).
35. L. J. Reed, H. Muench, A SIMPLE METHOD OF ESTIMATING FIFTY PER CENT ENDPOINTS. *American Journal of Epidemiology* **27**, 493-497 (1938).
36. S. Zaqout, L. L. Becker, A. M. Kaindl, Immunofluorescence Staining of Paraffin Sections Step by Step. *Front Neuroanat* **14**, 582218 (2020).
37. J. Schindelin *et al.*, Fiji: an open-source platform for biological-image analysis. *Nat Methods* **9**, 676-682 (2012).
38. M. A. Parish *et al.*, Pregnancy Reduces COVID-19 Vaccine Immunity Against Novel Variants. *medRxiv*, (2025).

Acknowledgments: We are grateful for the animal care staff that assisted with animals from the Miller Research Building Animal Facilities at Johns Hopkins University. Light microscopy images were generated using the instruments and support of the Light Microscopy Core of the Department of Molecular Microbiology and Immunology at the Johns Hopkins Bloomberg School of Public Health. We are also thankful for the histology laboratory personnel at the Johns Hopkins Oncology Tissue Services, and the Klein, Davis, and Thompson lab members for discussions about these data. We would also like to acknowledge Ryan Lewandowski for his technical assistance of digital histology scans at Michigan State University.

Funding: Funding provided the National Institutes of Health NIAID Johns Hopkins Center of Excellence for Influenza Research and Response (75N93021C00045; AP and SK), NIH/NIAID F32HD117584 (BS) and the NIH/NIAID 5T32AI007417-29 (MP).

Author contributions:

Conceptualization: BAS, MAP, AP, SLK

Methodology: BAS, LC, ASB, RJW, JRH, AP, SLK

Investigation: BAS, MAP, SNT, TZ, SC, JAL, JS

Visualization: BAS, JRH

Funding acquisition: SLK, AP

Project administration: SLK

Supervision: JRH, AP, SLK

Writing – original draft: BAS, JRH, AP, SLK

Writing – review & editing: All authors

Competing interests: Authors declare that they have no competing interests.

Data and materials availability: All data are available in the main text or the supplementary materials.

Supplementary Materials

1. Materials and Methods
2. Figs. S1-S7
3. References only cited in the Supplementary Materials (#30-38)

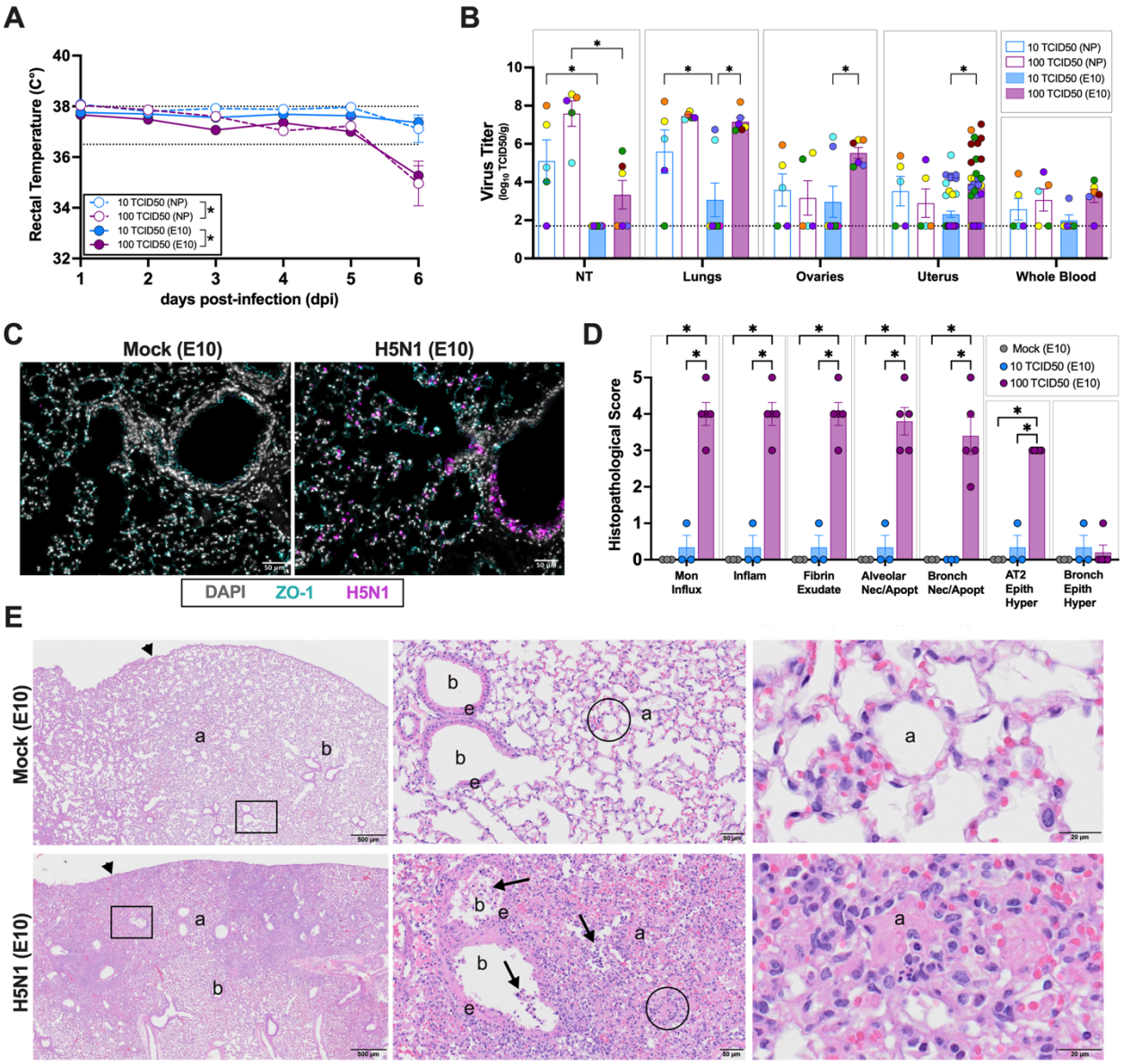

Fig. 1. Pathogenesis of bovine H5N1 in non-pregnant and pregnant (second-trimester equivalent gestation) female mice. CD-1 non-pregnant (NP; 7-8 weeks of age; n=5 per group) or pregnant (embryonic day 10 (E10); n=6-7 per group) female mice were intranasally inoculated with 10 or 100 TCID50 of H5N1 (A/bovine/OH). Mock controls were inoculated with media alone. (**A**) Rectal temperature was recorded daily as a measure of morbidity. The dashed line represents the rectal temperature range for a healthy mouse. (**B-E**) At 6 days post-infection, a subset of mice (n=5-7) from each group were euthanized and tissues were collected for downstream analysis. (**B**) Infectious virus was quantified by TCID50 assay in the nasal turbinates, lungs, ovaries, and whole blood of non-pregnant and pregnant dams. Individual points are color-coded by animal, while bar colors indicate group. (**C**) Immunofluorescent staining of fixed lung tissue (mock – left, and 100 TCID50 – right) from E10 pregnant dams. Cell nuclei (DAPI) are labeled in grey, tight junctions (ZO-1) to distinguish structural features are labeled in cyan, and

H5N1 virus protein is labeled in magenta. (**D**) Severity of individual lesions (histopathology) in lung tissue from E10 pregnant dams was scored by a board-certified pathologist for monocyte influx (Mon Influx), inflammation (Inflam), fibrin exudate, alveolar necrosis and apoptosis (Alv Necr Apopt), bronchiolar necrosis/apoptosis (Bronch Necr/Apopt), AT2 epithelial hyperplasia (AT2 Epith Hyper), and bronchiolar epithelial hyperplasia (Bronch Epith Hyper). (**E**) Light photomicrographs of hematoxylin and eosin–stained lung tissue taken at three different magnifications (low, medium and high) from right to left, respectively. Squares and circles indicate the location of magnified images to the right. Arrows in the lower middle photo highlight virus-induced inflammatory cell exudate in airway and alveolar airspaces ─ a, alveoli and b, bronchiole. Arrows in the right lower photo highlight the presence of apoptotic epithelial cells and apoptotic bodies lining alveolar septa, with accumulation of mixed inflammatory cells and proteinaceous fluid in alveolar lumens. Individual symbols (A) or bars (B and D) represent the mean ± standard error of the mean per group. Significant differences ($p < 0.05$) were determined by a repeated measures two-way ANOVA with Bonferroni post-hoc test (A) or two-way ANOVA with Bonferroni post-hoc test (B and D) and are indicated by an asterisk (*).

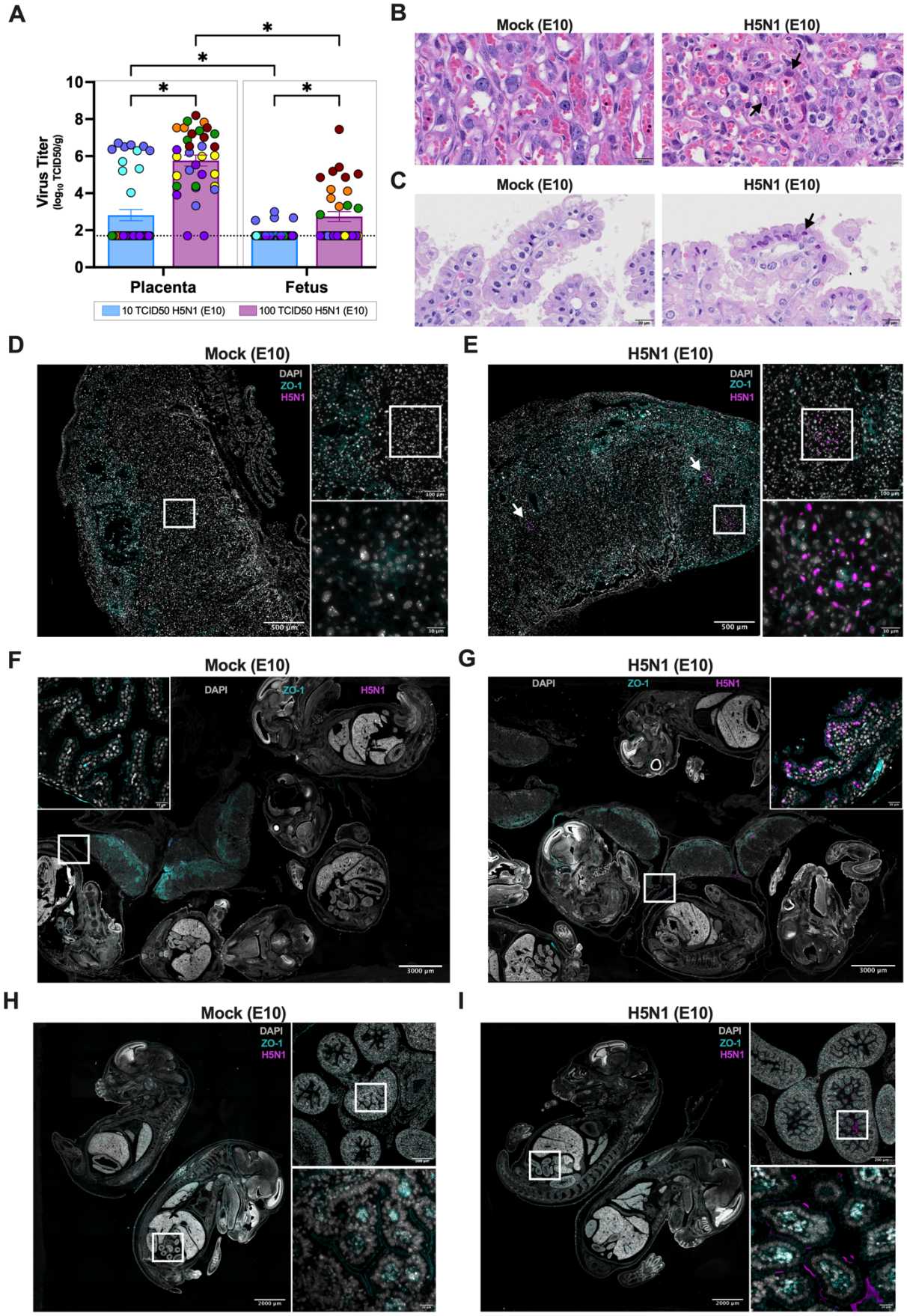
A
Virus Titer
(log10 TCID50/g)
10
8
6
4
2
0
Placenta
Fetus
10 TCID50 H5N1 (E10)
100 TCID50 H5N1 (E10)
B
Mock (E10)
H5N1 (E10)
C
Mock (E10)
H5N1 (E10)
D
Mock (E10)
DAPI
ZO-1
H5N1
500 µm
E
H5N1 (E10)
DAPI
ZO-1
H5N1
500 µm
F
Mock (E10)
DAPI
ZO-1
H5N1
3000 µm
G
H5N1 (E10)
DAPI
ZO-1
H5N1
3000 µm
H
Mock (E10)
DAPI
ZO-1
H5N1
2000 µm
I
H5N1 (E10)
DAPI
ZO-1
H5N1
2000 µm

Fig. 2. *In utero* vertical transmission and conceptus tissue tropism of bovine H5N1. CD-1 pregnant (embryonic day [E] 10) dams were intranasally inoculated with media (mock), 10 TCID50, or 100 TCID50 of H5N1 (A/bovine/OH). (**A**) At 6 days post-infection, a subset of mice (n= 5-7) from each group were euthanized, and infectious virus was quantified by TCID50 assay in a subset of placental and fetal tissues (n= 4-6/dam). The dashed line indicates the limit of detection. Individual points are color-coded by litter corresponding to the color of the dam in Fig. 1, while bar colors indicate viral dose. (**B, C**) Light photomicrographs of hematoxylin and eosin–stained placental and yolk-sac tissue from E10 pregnant dams. (**B**) Placental labyrinth of pregnant dams that were mock infected (controls) or inoculated with H5N1 (100 TCID50). (**C**) Yolk sac from pregnant dams mock infected or inoculated with H5N1 (10 TCID50). Arrows represent virus-associated, small focal lesions. Immunofluorescent staining of the placenta (**D–E**), conceptus (**H-I**), and fetus (**F–G**) from E10 pregnant dams inoculated with media (**D, H, F**) or H5N1 (100 TCID50; **E, G, I**). The left images were taken at 4X (**D**) or 4X tiled images (**F-H**). Higher-resolution images were captured at 20X (**D** and **E**; top right) or 10X (**H** and **I**; top right) and/or 60X (**D-E** and **H-I**; bottom right). The small panel in **F-G** was captured at 40X. White boxes indicate the regions displayed in the magnified images. Cell nuclei (DAPI) are shown in grey, tight junctions (ZO-1) to distinguish structural features are shown in cyan, and H5N1 whole virus antigen in magenta. Bars (A and B) represent the mean ± standard error of the mean per group, with individual mice indicated by colored points. Significant differences ($p < 0.05$) were determined by a two-way ANOVA with Bonferroni post-hoc test (A-B) and are indicated by an asterisk (*).

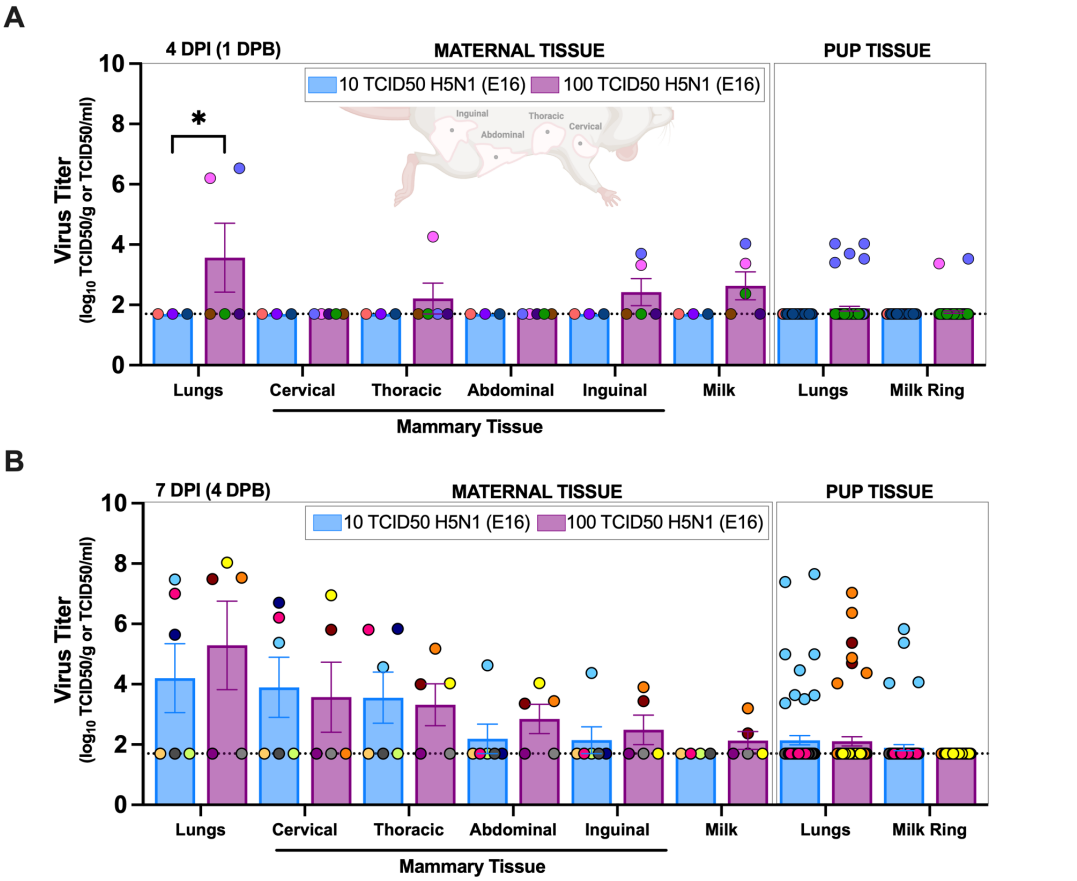
A
4 DPI (1 DPB)
MATERNAL TISSUE
PUP TISSUE
10 TCID50 H5N1 (E16)
100 TCID50 H5N1 (E16)
Virus Titer
(log10 TCID50/g or TCID50/ml)
Lungs
Cervical
Thoracic
Abdominal
Inguinal
Milk
Lungs
Milk Ring
Mammary Tissue
B
7 DPI (4 DPB)
MATERNAL TISSUE
PUP TISSUE
10 TCID50 H5N1 (E16)
100 TCID50 H5N1 (E16)
Virus Titer
(log10 TCID50/g or TCID50/ml)
Lungs
Cervical
Thoracic
Abdominal
Inguinal
Milk
Lungs
Milk Ring
Mammary Tissue

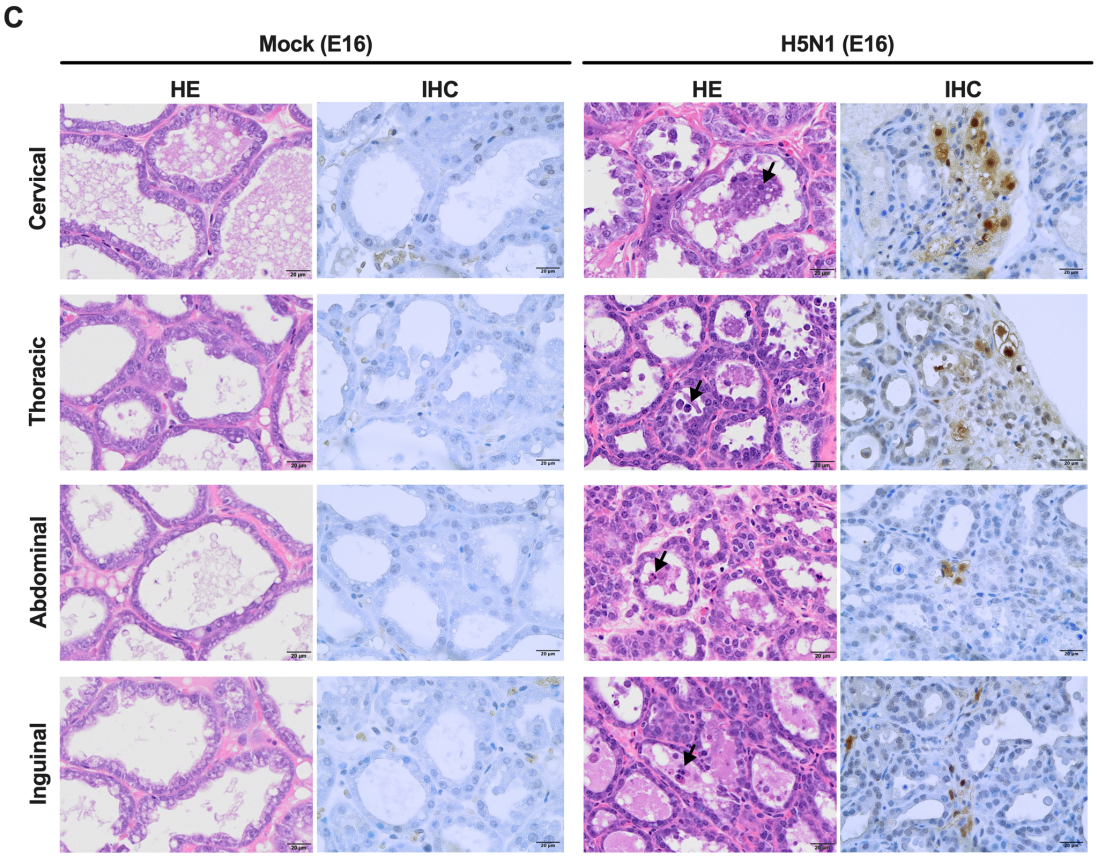
C
Mock (E16)
H5N1 (E16)
HE
IHC
HE
IHC
Cervical
Thoracic
Abdominal
Inguinal

Fig. 3. Post-birth vertical transmission and tissue tropism of bovine H5N1. CD-1 pregnant (embryonic day [E] 16) females were intranasally inoculated with 10 or 100 TCID50 of H5N1 (A/bovine/OH) or media (mock). At (**A**) 4 days post-infection (1-day post-birth) or (**B**) 7 days post-infection (4 days post-birth), a subset of dams and their entire litters were euthanized. Infectious virus was quantified by TCID50 assay in the lungs, milk, and mammary tissue (cervical, thoracic, abdominal, and inguinal) of lactating dams, as well as in the pup lungs and milk ring. Individual points are color-coded by litter. (**C**) Light photomicrographs of hematoxylin and eosin–stained (HE) mammary tissue sections collected 7-8 dpi from E16 pregnant dams (mock – left and 100 TCID50 – right). Arrows indicate pyknotic or karyorrhectic nuclei. Immunohistochemistry (IHC) staining for viral N1 antigen of fixed cervical, thoracic, abdominal, and inguinal mammary tissue (mock – left, and 100 TCID50 – right). Illustration depicting the collection sites for the various mammary tissues was created in BioRender. Seibert, B. (2025) https://BioRender.com/tq8un5s. Significant differences ($p < 0.05$) were determined by a two-way ANOVA with Bonferroni post-hoc test (A-B) and are indicated by an asterisk (*).

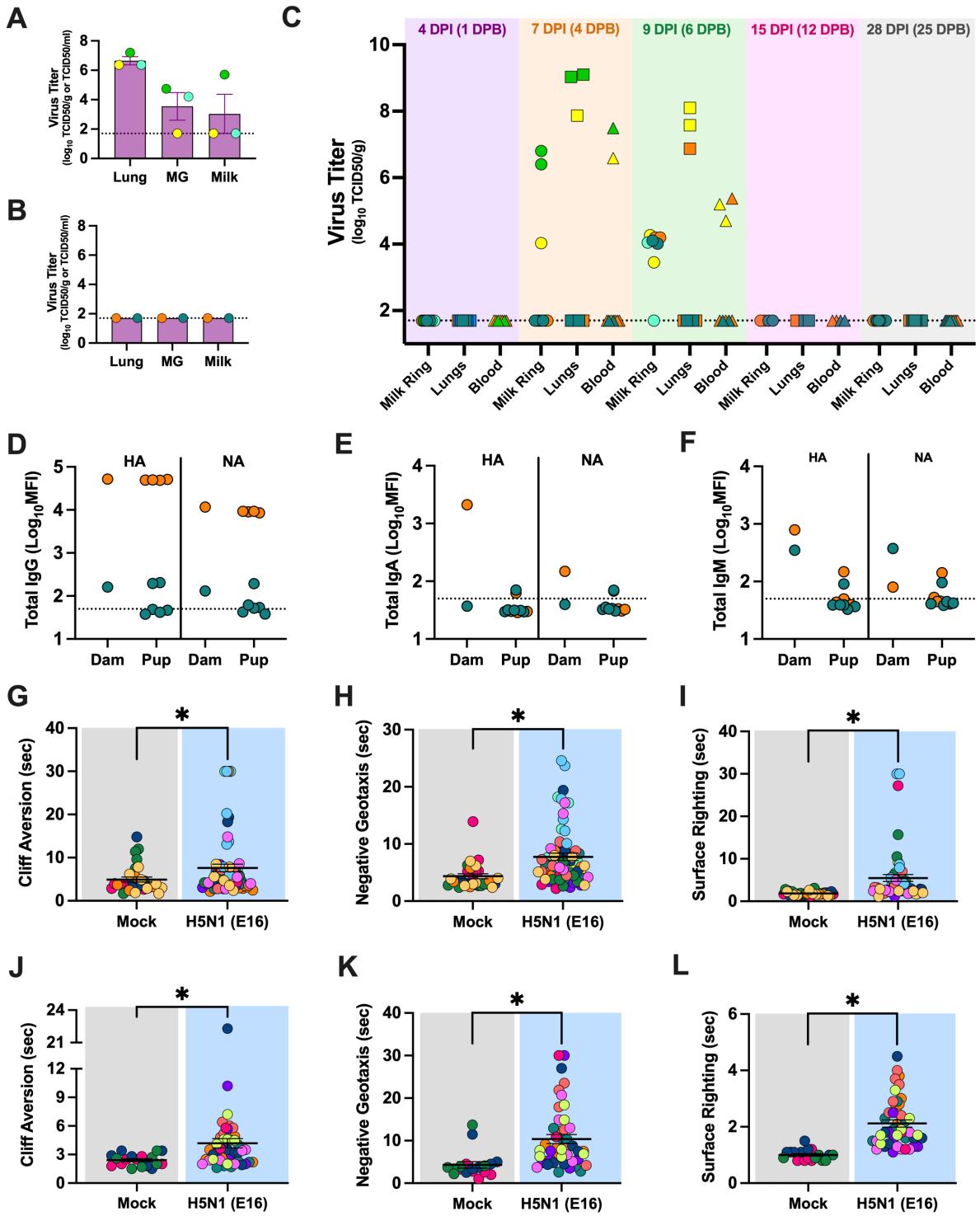

Fig. 4. Impact of post-birth bovine H5N1 virus transmission on offspring. CD-1 pregnant (embryonic day 16) dams were anaesthetized and intranasally inoculated with media (mock) or 10 TCID50 of H5N1 (A/bovine/OH). Between (**A**) 4-6 and (**B**) 28 days post-infection, a subset of dams was euthanized, and infectious virus was quantified by TCID50 assay in the lungs, mammary glands (MG), and milk. The dashed line indicates the limit of detection. (**C**) A subset of pups (n= 4-10) was euthanized at 4 days post-infection (dpi) (1 days post-birth (dpb)), 7 dpi (4 dpb), 9 dpi

(6 dpb), 15 dpi (12 dpb), and 28 dpi (25 dpb) and tissues, including the milk ring, lung, and whole blood, were collected and analyzed for infectious virus by TCID50 assay. The dashed line indicates the limit of detection. Individual points are color-coded by individual dam and their corresponding pups. H5N1 HA and NA specific (**D**) IgG, (**E**) IgA, and (**F**) IgM were measured in serum from dams and their corresponding pups euthanized at 28 dpi (25 dpb) using systems serology. The results are reported as $\log_{10}$ mean fluorescence intensity (MFI). The dashed line indicates the limit of assay background. Individual points are color-coded by individual dam and their corresponding pups. At 5 (**G-I**) and 9 (**J-L**) dpb, a subset of pups was assessed for cliff aversion (G and J), negative geotaxis (H and K), and surface righting (I and L) to measure neurological development. Individual points are color-coded by litter, with shaded colors indicating group: grey for media and blue for 10^1 TCID50-inoculated pregnant dams. Bars (A-B, G-L) represent the mean ± standard error of the mean per group, with individual mice indicated by points. Significant differences ($p < 0.05$) were determined by a two-tailed unpaired t-test (G-L) and are indicated by an asterisk (*).